Progress In Electromagnetics Research B, Vol. 35, 213–239, 2011

ANALYSIS AND DESIGN OF UNIVERSAL COMPACT FLEXIBLE UHF RFID TAG ANTENNA

T. G. Abo-Elnaga [1, *], E. A. F. Abdallah [1], and H. El-Hennawy [2]

[1]Electronics Research Institute, Cairo, Egypt

[2]Faculty of Engineering, Ain Shams University, Cairo, Egypt

Abstract—The main goal of this paper is to present a design procedure for a flexible compact universal UHF RFID tag antenna suitable for worldwide UHF RFID applications. Systematic design procedure is introduced through the derivation of dipole input impedance general relation using induced EMF method considering wire radius effect. T-matched chart is used to match the tag input impedance with the chip input impedance and finally develop a flow chart to summarize the design procedure. The proposed antenna compactness trend is achieved through applying meandering and Franklin shape to conventional printed dipole antenna. Flexibility trend is achieved through using liquid crystal polymer LCP material as antenna substrate. The proposed antenna covers the frequency band 865 MHz to 1078 MHz and occupies an area of 1306.6 mm^2. The computed radar cross section RCS and conjugate match factor CMF insure that the proposed antenna structure is easily detectable and achieves acceptable matching level. Power reflection coefficient PRC is computed, measured and good agreement is obtained. Other antenna parameters such as radiation efficiency, gain and radiation pattern are also calculated. The proposed antenna is cheap, flexible and suitable for UHF RFID universal application.

1. INTRODUCTION

RFID system mainly consists of two components, namely reader and tag. Reader broadcast queries to tag in its wireless transmission range for information contained in tag and the tag will reply with required information. RFID is an extremely important technology of

Received 11 September 2011, Accepted 27 October 2011, Scheduled 31 October 2011

* Corresponding author: Tamer Gaber Abo-Elnaga (tgaber010@yahoo.com).

automatic identification. It is being used in a wide range of applications such as electronic toll collect (ETC), vehicle access, electronic article surveillance (EAS), animal tagging, supply chain tracking, warehouse management, and security systems. RFID systems operating at UHF frequencies have received considerable attention for various commercial applications, such as supply chain management or inventory control. In this regard, a great demand of UHF RFID system is expected to replace the current position of barcode system. Different frequencies ranges are adopted in different countries at UHF frequencies such as 920.5–924.5 MHz in China, 920–926 MHz in Australia, 866–869 MHz and 920–925 MHz in Singapore, 952–955 MHz in Japan and 902–928 MHz in USA, Canada, Mexico, Puerto Rico, Costa Rica, Latin America, etc. [1–4].

The motivations of this paper is to introduce a flexible universal UHF RFID tag suitable for RFID applications all over the world, develop a systematic procedure to match the tag input impedance to RFID chip, develop general relation to predict the dipole input impedance and finally achieve reasonable size reduction. The proposed antenna achieves the universal UHF RFID operation through covering the frequency band from 865 MHz to 1078 MHz. Flexibility trend is achieved through choosing liquid crystal polymer LCP substrate for the proposed antenna fabrication which is a fairly new and promising thermoplastic organic material that provides very reliable high-performance at low cost. T-matched chart is used to match the tag input impedance with the chip input impedance, and a flow chart is developed to systemize the design procedure as shown in Fig. 1. The details of the design procedure are explained through different sections of this paper. A general dipole input impedance relation is obtained using the induced EMF method taking the wire radius effect into account, and the relation is verified through comparison with previous published results. Compactness is achieved through designing conventional dipole antenna, meander dipole antenna MDA with derivation of its resonance frequency and Franklin shape dipole antenna which occupies a total area of 1306.6 mm^2 compared with U-shaped slot tag antenna with geometry that occupies 3600 mm^2 [5], proximity-coupled feed RFID tag antenna with 1838.55 mm^2 [6], U-shaped RFID tag antenna with 2912 mm^2 [7], RFID tag antenna using compact artificial magnetic conductor AMC substrate with total area of 2307.48 mm^2 [8], microstrip patch antenna with EBG ground plane with area of 10000 mm^2 [9], inductively coupled loop antennas with area of 2551.5 mm^2 [10] and bow tie C shape feeding scheme tag antenna which occupies an area of 33000 mm^2 [11].

The proposed antenna is fabricated over LCP material with

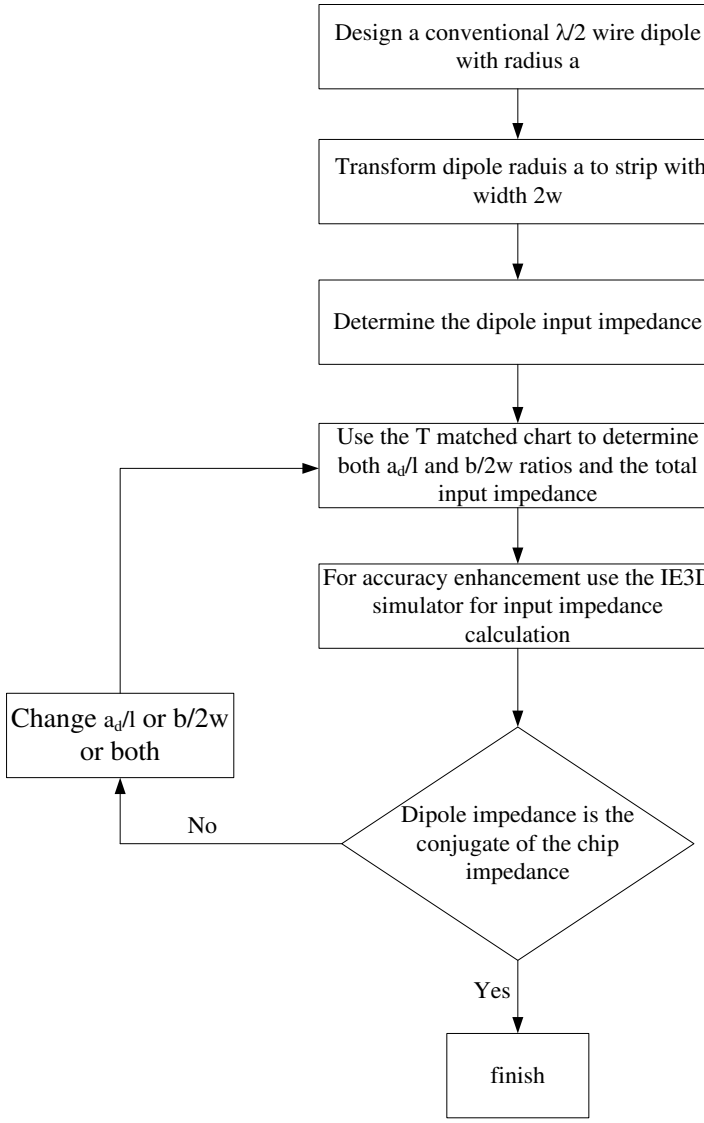

Figure 1. Design procedure flow chart for the dipole antenna with T-matched circuit.

dielectric constant $\varepsilon_r = 2.9$, height of 0.05 mm and loss tangent $\tan\delta = 0.0025$. Computed radar cross section RCS and conjugate match factor CMF are considered. Power reflection coefficient PRC is computed, measured, and discussed. Other antenna parameters such

as radiation efficiency, gain and radiation pattern are obtained and discussed. The paper is organized as follows. Section 2 introduces the general induced EMF derivation and verification. T-matched chart concept is discussed in Section 3. Resonant frequency of meander dipole antenna is introduced and discussed in Section 4. Finally, numerical and experimental results are introduced and discussed through the design of conventional dipole antenna, meander dipole antenna and Franklin shape dipole antenna. Derived relations together with the IE3D Zeland MoM based ready made simulator are used.

2. ANALYSIS OF FINITE LINEAR DIPOLE INPUT IMPEDANCE USING EMF METHOD

The induced EMF method is the technique adopted to derive closed-form expressions for the input impedance of finite linear dipole with length l and radius a, through the calculation of the current distribution and tangential electric field E_z along the surface of the wire. It should be noted that this simple configuration is used just to describe the physics related to the dipole impedance. In general, the vector potential $\mathbf{A}$ is given as [12]:

$$\mathbf{A}(x,y,z) = \frac{\mu}{4\pi}\int_C I_e\left(x',y',z'\right)\frac{e^{-jkR}}{R}dl' \tag{1}$$

where (x,y,z) represent the observation point coordinates, I_e the electric current, (x',y',z') the coordinates of the source, and R the distance from any point on the source to the observation point. Path C is along the length of the source. For a very thin dipole, the current distribution is based on the fact that the antenna is center-fed and that the current vanishes at the end points ($z' = \pm\frac{l}{2}$) and can be written

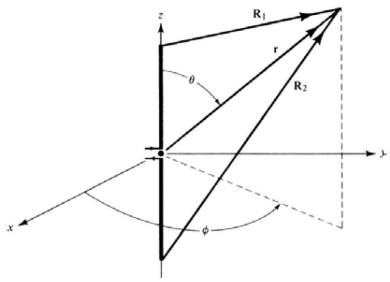

Figure 2. Dipole geometry.

as

$$I_e\left(x'=0,y'=0,z'\right) = \begin{cases} \hat{a}_z I_o \sin\left[k\left(\frac{l}{2}-z'\right)\right], & 0 \le z' \le l/2 \\ \hat{a}_z I_o \sin\left[k\left(\frac{l}{2}+z'\right)\right], & -l/2 \le z' \le 0 \end{cases} \quad (2)$$

$$\mathbf{H} = \frac{1}{\mu}\nabla \times \mathbf{A} = -\hat{a}_\emptyset \frac{1}{\mu}\frac{\partial A_z}{\partial \rho} \quad (3)$$

Using the vector potential $\mathbf{A}$ with thin wire approximation and Cartesian to cylindrical coordinates transformation at $\phi = \frac{\pi}{2}$, the magnetic field $\mathbf{H}$ using Eqs. (1)–(3) can be written as Eq. (4)

$$\mathbf{H}=-\hat{a}_\emptyset \frac{1}{j8\pi} I_o \left[e^{jk\left(\frac{l}{2}\right)} \int_{-l/2}^{0} \frac{\partial}{\partial y}\frac{e^{-jk(R-z')}}{R}dz' - e^{-jk\left(\frac{l}{2}\right)} \int_{-l/2}^{0} \frac{\partial}{\partial y}\frac{e^{-jk(R+z')}}{R}dz' \right.$$
$$\left. + e^{jk\left(\frac{l}{2}\right)} \int_{0}^{l/2} \frac{\partial}{\partial y}\frac{e^{-jk(z'+R)}}{R}dz' - e^{-jk\left(\frac{l}{2}\right)} \int_{0}^{l/2} \frac{\partial}{\partial y}\frac{e^{-jk(R-z')}}{R}dz' \right] \quad (4)$$

where I_o is the maximum current. Representing the differential terms in Eq. (4) as:

$$\frac{\partial}{\partial y}\frac{e^{-jk(R-z')}}{R} = -jky\frac{e^{-jk(R-z')}}{R^2} - y\frac{e^{-jk(R-z')}}{R^3} \quad (5a)$$

$$\frac{\partial}{\partial y}\frac{e^{-jk(z'+R)}}{R} = -jky\frac{e^{-jk(z'+R)}}{R^2} - y\frac{e^{-jk(z'+R)}}{R^3} \quad (5b)$$

$$d\left[\frac{e^{-jk(R-z')}}{R\left(R-z'+z\right)}\right] = e^{-jk(R-z')}\left(jk\frac{1}{(R)^2}+\frac{1}{(R)^3}\right)dz' \quad (5c)$$

$$d\left[\frac{e^{-jk(z'+R)}}{R\left(R+z'-z\right)}\right] = e^{-jk(z'+R)}\left(-jk\frac{1}{(R)^2}-\frac{1}{(R)^3}\right)dz' \quad (5d)$$

Substitute Eq. (5) in Eq. (4) we get:

$$\mathbf{H} = -\hat{a}_\emptyset \frac{1}{j8\pi} I_o \left[-e^{jk\left(\frac{l}{2}\right)} y \int_{-l/2}^{0} d\left[\frac{e^{-jk(R-z')}}{R\left(R-z'+z\right)}\right] \right.$$
$$-e^{-jk\left(\frac{l}{2}\right)} y \int_{-l/2}^{0} d\left[\frac{e^{-jk(z'+R)}}{R\left(R+z'-z\right)}\right] + e^{jk\left(\frac{l}{2}\right)} y \int_{0}^{l/2} d\left[\frac{e^{-jk(z'+R)}}{R\left(R+z'-z\right)}\right]$$
$$\left. -e^{-jk\left(\frac{l}{2}\right)} y \int_{0}^{l} /2d\left[\frac{e^{-jk(R-z')}}{R\left(R-z'+z\right)}\right] \right] \quad (6)$$

Performing the integration referring to Fig. 1 and rearranging the terms we can get Eq. (7) as:

$$\mathbf{H} = -\hat{a}_{\emptyset}\frac{1}{j4\pi}I_o y\left[e^{-jk(R_2)}\left(\frac{1}{(R_2)^2-(+l/2+z)^2}\right)\right.$$
$$\left.-e^{-jk(r)}2\cos\left(k\left(\frac{l}{2}\right)\right)\left(\frac{1}{r^2-z^2}\right)+e^{-jk(R_1)}\left(\frac{1}{(R_1)^2-(-l/2+z)^2}\right)\right] \quad (7)$$

$$\mathbf{H} = -\hat{a}_{\emptyset}\frac{1}{j4\pi}I_o\frac{1}{y}\left[e^{-jk(R_2)} - 2e^{-jk(r)}\cos\left(k\left(\frac{l}{2}\right)\right) + e^{-jk(R_1)}\right] \quad (8)$$

From Maxwell's equations one can obtain E_z when using cylindrical coordinates as:

$$E_z = \eta\frac{-j}{4\pi}I_o\left[\frac{e^{-jk(R_2)}}{R_2} - 2\cos\left(k\left(\frac{l}{2}\right)\right)\frac{e^{-jk(r)}}{r} + \frac{e^{-jk(R_1)}}{R_1}\right] \quad (9)$$

Based on [12], one can calculate the induced potential and consequently the input impedance Z_a as in Eq. (10).

$$Z_m = -\frac{1}{I_o^2}\int_{-l/2}^{l} /2I_z\left(\rho = a, z = z'\right)E_z\left(\rho = a, z = z'\right)dz' \quad (10)$$

Using both Eqs. (2) and (9) Z_a can be written as in Eq. (11):

$$Z_a = \frac{\eta}{8\pi}e^{jk\left(\frac{l}{2}\right)}\int_{-l/2}^{0}\left[\frac{e^{jk(z'-R_2)}}{R_2} - 2\cos\left(k\left(\frac{l}{2}\right)\right)\frac{e^{jk(z'-r)}}{r} + \frac{e^{jk(z'-R_1)}}{R_1}\right]dz'$$
$$-\frac{\eta}{8\pi}e^{-jk\left(\frac{l}{2}\right)}\int_{-l/2}^{0}\left[\frac{e^{-jk(R_2+z')}}{R_2} - 2\cos\left(k\left(\frac{l}{2}\right)\right)\frac{e^{-jk(r+z')}}{r} + \frac{e^{-jk(R_1+z')}}{R_1}\right]dz'$$
$$+\frac{\eta}{8\pi}e^{jk\left(\frac{l}{2}\right)}\int_{0}^{l/2}\left[\frac{e^{-jk(R_2+z')}}{R_2} - 2\cos\left(k\left(\frac{l}{2}\right)\right)\frac{e^{-jk(r+z')}}{r} + \frac{e^{-jk(R_1+z')}}{R_1}\right]dz'$$
$$-\frac{\eta}{8\pi}e^{-jk\left(\frac{l}{2}\right)}\int_{0}^{l/2}\left[\frac{e^{jk(z'-R_2)}}{R_2} - 2\cos\left(k\left(\frac{l}{2}\right)\right)\frac{e^{jk(z'-r)}}{r} + \frac{e^{jk(z'-R_1)}}{R_1}\right]dz' \quad (11)$$

Using the following relations [13]

$$\begin{aligned} C_i(-ku_1) &= C_i(ku_1) - i\pi \\ S_i(-ku_1) &= -S_i(ku_1) \\ \int_{u_1}^{u_2} \frac{e^{jku}}{u} du &= [C_i(ku) + i\, S_i(ku)]|_{u_1}^{u_2} \end{aligned} \tag{12}$$

Using Eq. (12) in Eq. (11) one obtains Eq. (13):

$$\begin{aligned} Z_a = \frac{\eta}{4\pi} \Big[& \left(2 + 2e^{-jkl}\right) (-C_i(kx_2) + j\, S_i(kx_2)) \\ & + 2\left(1 + 2\cos^2\left(\frac{kl}{2}\right)\right) (C_i(kx_1) - j\, S_i(kx_1)) \\ & + \left(2 + 2e^{jkl}\right) (-C_i(kx_3) + j\, S_i(kx_3)) \\ & + \left(e^{jkl}\right) (C_i(kx_4) - j\, S_i(kx_4)) \\ & + \left(-e^{-jkl}\right) (-C_i(kx_5) + j\, S_i(kx_5)) \Big] \end{aligned} \tag{13}$$

where

$$R_1 = \sqrt{a^2 + \left(z' - \frac{l}{2}\right)^2}, \quad R_2 = \sqrt{a^2 + \left(z + \frac{l}{2}\right)^2}, \quad x_1 = a,$$

$$x_2 = \left(\sqrt{a^2 + \left(\frac{l}{2}\right)^2} - \frac{l}{2}\right), \quad x_3 = \left(\sqrt{a^2 + \left(\frac{l}{2}\right)^2} + \frac{l}{2}\right),$$

$$x_4 = \left(\sqrt{a^2 + l^2} + l\right) \text{ and } x_5 = \left(\sqrt{a^2 + l^2} - l\right)$$

It was assumed by [14] that the radius of the wire is negligible, and the input impedance is given by:

$$\begin{aligned} Z_a = \frac{\eta}{2\pi} \Bigg\{ & C + \ln(kl) - C_i(kl) + \frac{1}{2}\sin(kl)\,[S_i(2kl) - 2S_i(kl)] \\ & + \frac{1}{2}\cos(kl)\left[C + \ln\left(\frac{kl}{2}\right) + C_i(2kl) - 2C_i(kl)\right] \Bigg\} \\ & + j\frac{\eta}{4\pi} \{2S_i(kl) + \cos(kl)\,[2S_i(kl) - S_i(2kl)] \\ & - \sin(kl)\left[2C_i(kl) - C_i(2kl) - C_i\left(\frac{2ka^2}{l}\right)\right]\Bigg\} \end{aligned} \tag{14}$$

where

$$C = 577215665$$

$$C_i(x) = -\int_x^{\infty} \frac{\cos(\tau)}{\tau} d\tau$$

$$S_i(x) = \int_0^x \frac{\sin(\tau)}{\tau} d\tau$$

$$C_{in}(x) = \int_0^x \frac{1-\cos(\tau)}{\tau} d\tau = C + \ln(x) - C_i(x)$$

Based on Eq. (13) and Eq. (14), a matlab code is built, and the results are shown in Fig. 3. As shown in Fig. 3(a) good agreement is found for the impedance reactive part which is calculated using Eq. (13) and Eq. (14), noting that the curves are very close at wire radius equal to 0.0015λ and 0.00015λ. As shown in Fig. 3(b), as radius becomes less than 0.075λ all computed impedance resistive part curves using Eq. (13) or Eq. (14) are nearly the same. It should be mentioned that using Eq. (13), the resistive part of the wire dipole input impedance is $212.3\,\Omega$, $212.688\,\Omega$, $212.69226\,\Omega$ and $212.69232\,\Omega$ for radius a equals 0.075λ, 0.015λ, 0.0015λ, 0.00015λ, respectively. The maximum difference between the curves obtained by both equations at $l/\lambda = 0.9$ is about $10\,\Omega$ (which is approximately 5% from that obtained using Eq. (14)). This means that Eq. (13) is the general equation for calculating Z_a for any value of α, while Eq. (14) is a special case when a is very small as compared to wavelength.

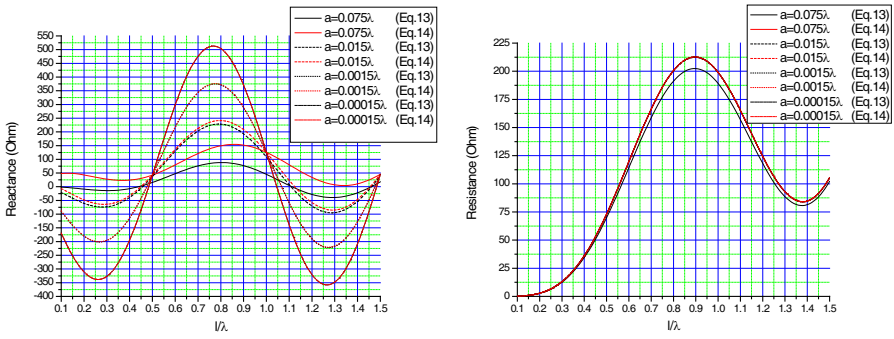

(a) (b)

Figure 3. (a) Dipole reactance versus normalized length $1/\lambda$ for different radii α using induced EMF method. (b) Dipole resistance versus normalized length l/λ for different radii a using induced EMF method.

3. IMPEDANCE MATCHING OF FINITE LINEAR DIPOLE-T-MATCHED CHART

In case of RFID tags the antenna has to be matched to the IC, and one typical method is T-matched circuit which is used to match the dipole input impedance Z_a to the chip input impedance. Referring to Fig. 4, the input impedance of a (planar) dipole of length l can be changed by introducing a centered short-circuited stub. The antenna source is connected to a second dipole of length $a_d \leq l$, placed at a close distance b from the first and larger ones. It can be proved that the impedance at the source point is given by [15]:

$$Z_{in} = \frac{2Z_t\,(1+\alpha)^2\,Z_a}{2Z_t + (1+\alpha)^2 Z_a} \tag{15}$$

where

$$\begin{aligned} Z_t &= jZ_0\,\tan\left(\frac{k\,a_d}{2}\right) \\ Z_0 &= 276\log_{10}\left(\frac{b}{\sqrt{r_e r'_e}}\right) \\ r_e &= 0.25(2w) \\ r'_e &= 0.25(2w') \end{aligned}$$

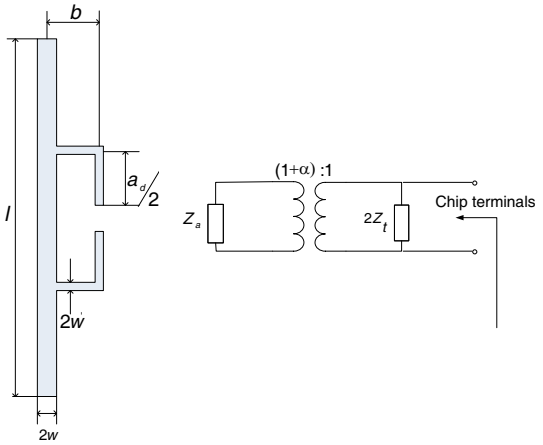

Figure 4. T-matched configuration for planar dipoles and equivalent circuit where the impedance step-up ratio $(1 + \alpha)$ is related to the conductors' cross-sections.

$$\alpha = \frac{\ln\left(\frac{b}{r'_e}\right)}{\ln\left(\frac{b}{r_e}\right)}$$

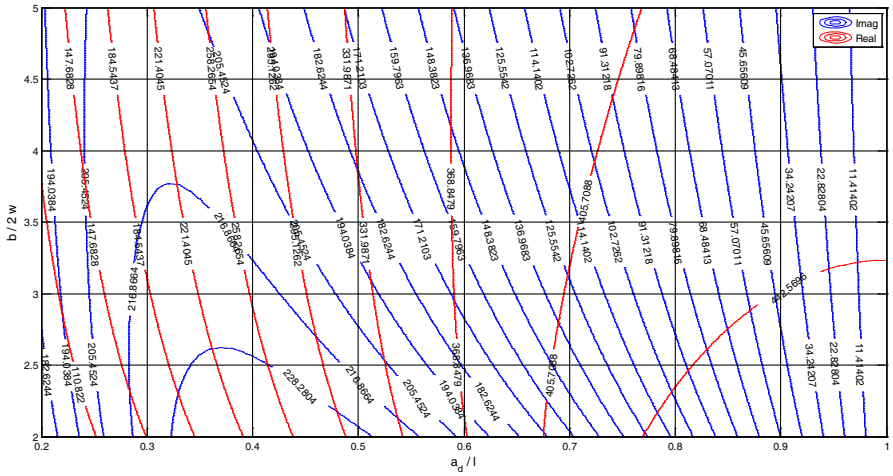

(a)

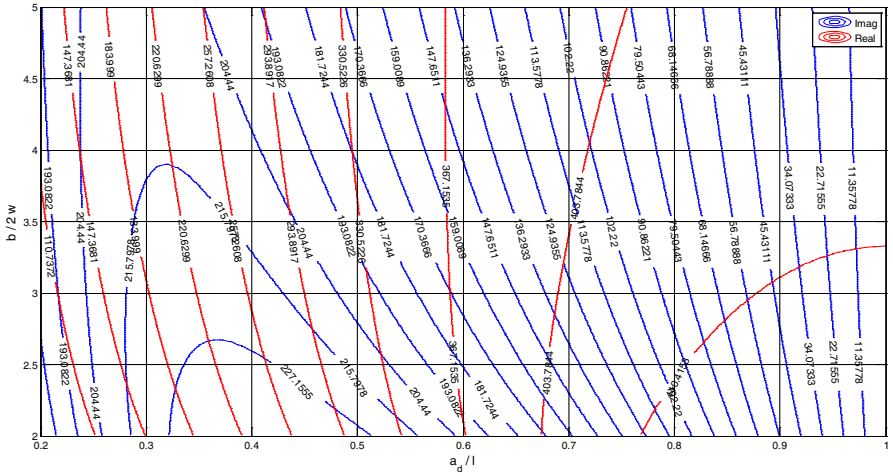

(b)

Figure 5. (a) T match circuit chart for $\lambda/2$ dipole with 75 ohm input impedance [15]. (b) T match circuit chart for $\lambda/2$ dipole with 75 ohm input impedance [16].

the parameters appeared in Eq. (15) was replaced according to [16] as follows:

$$\begin{aligned} Z_0 &= \frac{\eta}{\pi}\cosh^{-1}\left(\frac{b/2}{\sqrt{r_e r'_e}}\right) \\ \alpha &= \frac{\cosh^{-1}\left(\frac{v^2-u^2+1}{2v}\right)}{\cosh^{-1}\left(\frac{v^2+u^2-1}{2uv}\right)} \\ u &= \frac{w}{w'} \\ v &= \frac{b}{0.25(2w')} \end{aligned} \tag{16}$$

For verification, Eqs. (15) and (16) are applied on a $\lambda/2$ dipole with input impedance Z_a of $75\,\Omega$ and $u = w/w' = 3$ [15], we can plot an impedance chart for the T-matched circuit as shown in Figs. 5(a) and 5(b), respectively. It should be noted that both Figs. 5(a) and Fig. 5(b) are almost typically the same which indicates that the analyses of [15, 16] are correct and give approximately identical curves, but the numerical calculations published in [15] is not correct.

4. IMPEDANCE MATCHING OF MORE COMPLEX ANTENNA GEOMETRIES

The resonance frequency of the dipole antenna changes if the geometry is changed, and this fact is illustrated by a meander dipole. Fig. 6 shows two meander lines dipole antenna which could be represented by a twin lines with a short circuited termination which could be used to represent the two parallel real lines. The bold real line and dashed line are considered as a straight conducting line with total length S_m and diameter b_m [14].

The resonant frequency of the MDA could be represented by the following equation [14]:

$$\begin{aligned} \frac{\mu_o\lambda}{4\pi}\left(\log\frac{2\lambda}{b_m}-1\right) &= \frac{\mu_o}{2\pi}S_m\left(\log\frac{4S_m}{b_m}-1\right) \\ &\quad + m\frac{\mu_o h_m}{\pi}\log\left(\frac{2W_m}{b_m}\right)\left(1+\frac{1}{3}\left(kh_m\right)^2\right) \end{aligned} \tag{17}$$

where, W_m is the distance between twin lines, h_m the twin lines height, k equal to $2\pi/\lambda$ and μ_o the vacuum permeability. For verification purpose, we recalculate Eq. (17) with $S_m = 129\,\text{mm}$, $b_m = 1\,\text{mm}$, $h_m = 10\,\text{mm}$ and $W_m = 6\,\text{mm}$ and plot a graph for amount of meander

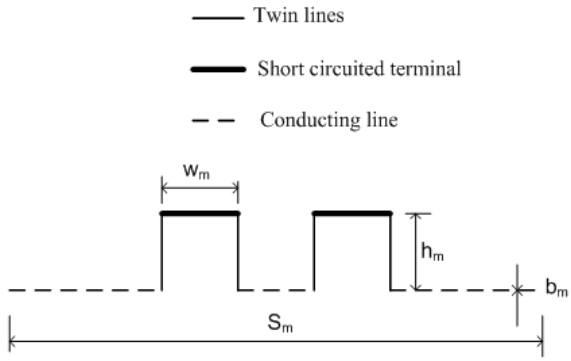

Figure 6. Meander line dipole antenna.

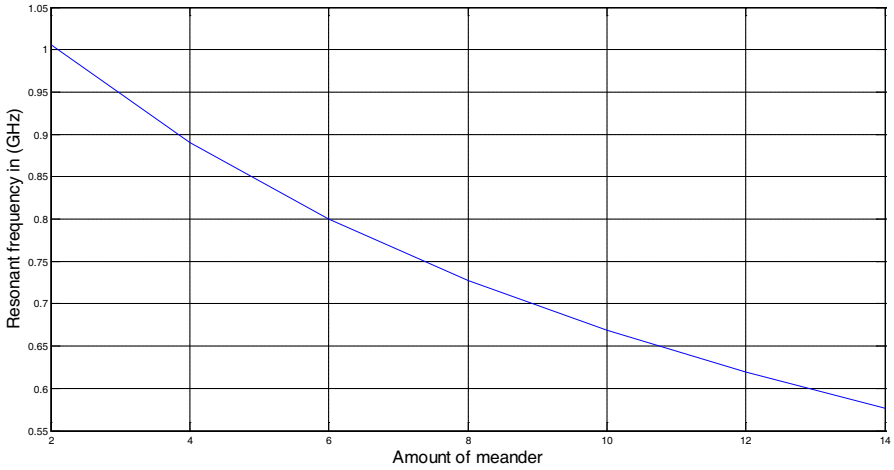

Figure 7. Resonant frequencies versus meander's number (S_m = 129 mm, $b_m = 1$ mm, $h_m = 10$ mm and $W_m = 6$ mm).

and the resonance frequency as shown in Fig. 6 which agrees well with that published in [14].

For compactness requirements and after many trials, we can start with $S_m = 72.6$ mm, $b_m = 1$ mm and $W_m = 18$ mm, $m = 2$ and using Eq. (17) to calculate h_m to achieve 900 MHz as resonant frequency as given in Table 1. As clear from this table that the required resonant frequency (900 MHz) can be achieved for a value of h_m which lies between 28 mm and 30 mm.

Table 1. The value of h_m to achieve resonant frequency $f_o = 900\,\text{MHz}$.

h_m (mm)	Resonant frequency (GHz)
20	1.0906
22	1.0411
24	0.9959
26	0.9544
28	0.9163
30	0.8812

5. DESIGN AND SIMULATION OF DIPOLE TAGS

In this section, we investigate the design process by three case studies. At first we examine finite linear dipole. In order to reduce tag size, we evaluate two more complex geometries: Meander dipole and Franklin dipole.

5.1. Finite Linear Dipole

Since RFID tags could be placed on differently shaped objects such as boxes, cylindrical bins, vehicles, etc. and no extra packaging will be around the RFID tag, LCP substrate is considered one of the best candidate substrates for RFID tag antenna. A prototype $\lambda/2$ dipole antenna is designed on a LCP substrate ($\varepsilon_r = 2.9$, thickness of $50\,\mu\text{m}$ and $\tan\delta = 0.0025$) and resonant frequency $f_r = 900\,\text{MHz}$ for UHF RFID system. The wire radius is chosen for fabrication purpose to be 0.0015λ. The input impedance of $\lambda/2$ dipole as predicted by Eq. (13) and Eq. (14) is found to be $73.129 + \text{j}42.54\,\Omega$. Using [17], the radius a could be transformed to strip of width $2w = 0.006\lambda$. The feed gap width is chosen to be 1 mm which is suitable for the RFID chip dimensions. The dipole geometry is shown in Fig. 8(a). The structure is simulated using IE3D, and the dipole input impedance versus frequency is shown in Fig. 8(b) which indicates that at 900 MHz the dipole input impedance equals $89.91 + \text{j}43.58\,\Omega$. This difference is due to the transformation from wire structure into planar structure. As given by [18], the chip input impedance equals $13.9 - \text{j}143.6\,\Omega$. It should be mentioned that the operating frequency for the chip will cover the band from 860 MHz to 960 MHz, and its input impedance varies from $15.69 - \text{j}152.6\,\Omega$ at 860 MHz to $12.61 - \text{j}137\,\Omega$ at 960 MHz. Applying Eq. (15) at a $\lambda/2$ dipole with input impedance Z_a of $89.91 + \text{j}43.58\,\Omega$ and $w/w' = 1$ at 900 MHz, we can plot an impedance chart for the

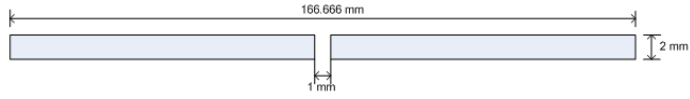

(a)

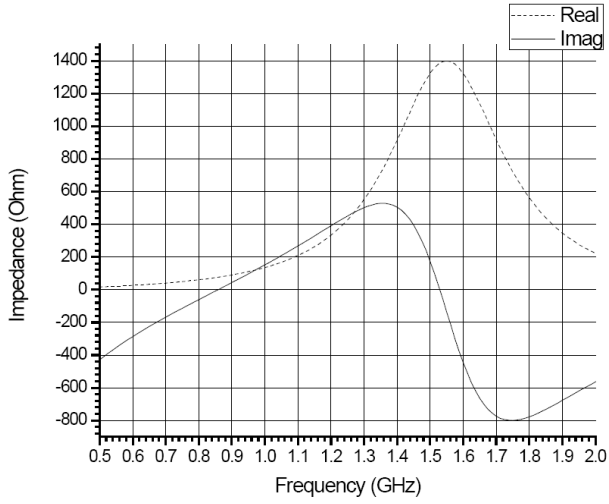

(b)

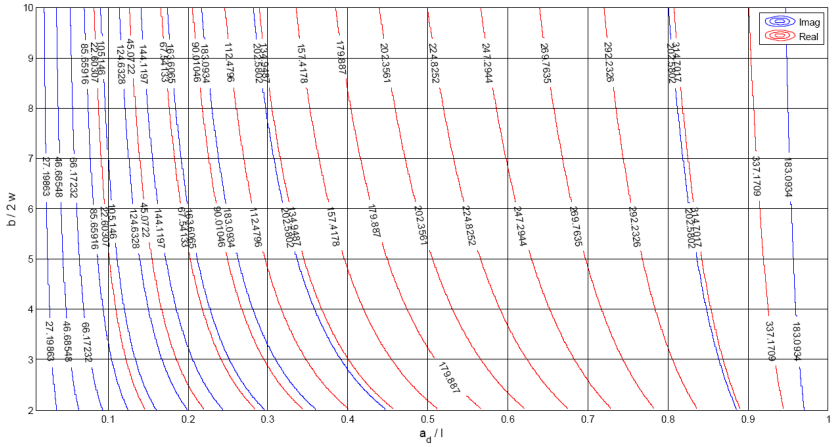

(c)

Figure 8. (a) Printed $\lambda/2$ dipole at 900 MHz. (b) The $\lambda/2$ dipole input impedance versus frequency at 900 MHz. (c) T-matched circuit chart for $\lambda/2$ dipole with $89.91 + \mathrm{j}43.58\,\Omega$ input impedance.

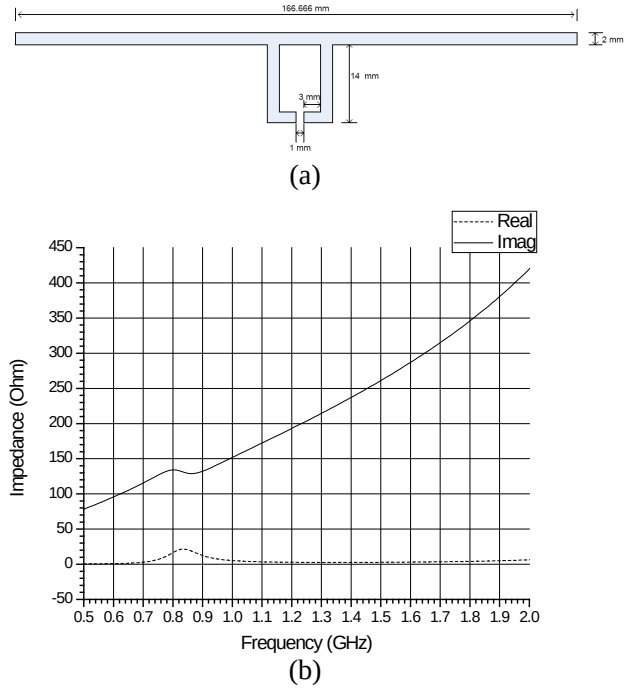

Figure 9. (a) $\lambda/2$ dipole with T-matched circuit for $13.9 - \mathrm{j}143.6\,\Omega$ chip input impedance. (b) $\lambda/2$ dipole with T-matched circuit input impedance versus frequency.

T-matched circuit as shown in Fig. 8(c). As a starting point, we can choose $b/w = 7$ and $a_d/l = 0.1$ which, from Fig. 8(c), give total input impedance of approximately $28 + \mathrm{j}105\,\Omega$. As shown in Fig. 9(a), the structure is simulated using IE3D simulator. Both b/w and a_d/l are optimized to be 7 and 0.048, respectively, which drive input impedance to be $12.45 + \mathrm{j}132.1\,\Omega$ as shown in Fig. 9(b). A flow chart is shown in Fig. 10 which summarizes the design procedure for the printed dipole and how the conjugate match is done using the T-matched method. Since the RFID tag is designed to provide an impedance match between two components with complex impedances, the power reflection coefficient (PRC) is used to determine the bandwidth of the RFID tag antenna by using the criterion PRC $< -3\,\mathrm{dB}$ [11]. As shown in Fig. 10(a), the $\lambda/2$ printed dipole covers the frequency band 750 MHz–1025 MHz which is suitable for the universal UHF RFID applications. Other two important parameters should be considered which are radar cross section RCS and conjugate match factor CMF.

RCS is a measure of how detectable an object is with a transmitter. Larger RCS indicates that an object is more easily detected. As shown in Fig. 10(b), at 900 MHz the antenna introduces $0.0588\,\mathrm{m}^2$ which makes its detection an easy task for the reader. CMF is used to judge how good an RFID antenna is matched in the reality and equals 1 at perfect conjugate matching between the tag and the chip input impedance. As shown in Fig. 10(c), CMF = 0.77 at 900 MHz which indicates that there is a good matching between the tag and chip. Fig. 10(d) shows the radiation pattern which is almost omnidirectional at the H-plane and the shape of 8 at the E-plane which makes this pattern very suitable for the RFID surveillance applications. Other antenna parameters such as conjugate match gain and radiation efficiency are shown in Fig. 10(e) and Fig. 10(f), respectively.

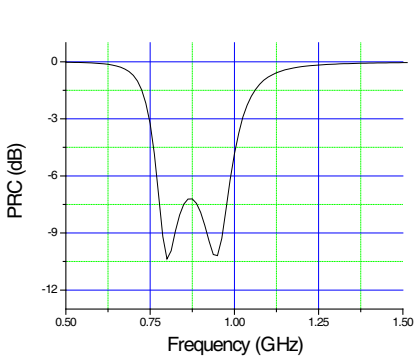

(a)

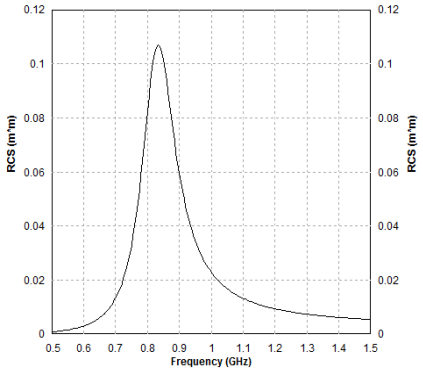

(b)

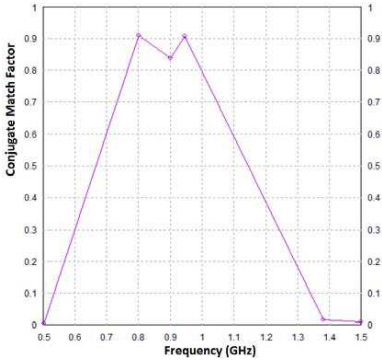

(c)

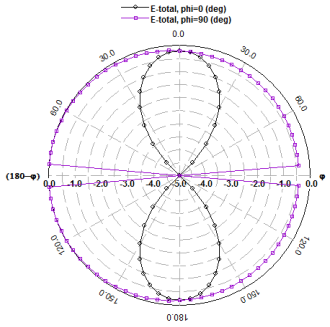

(d)

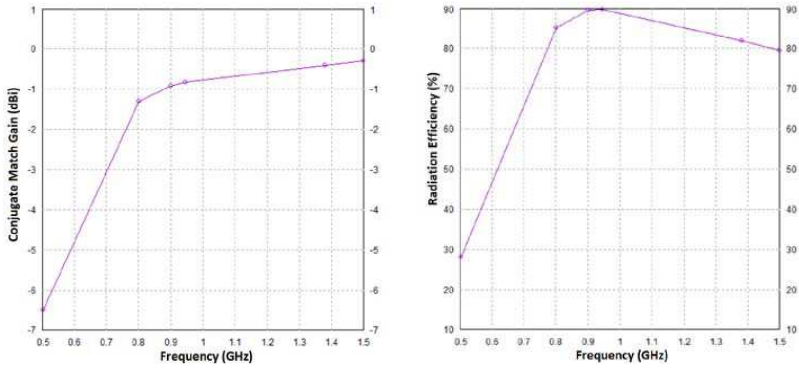

(e) (f)

Figure 10. (a) PRC of printed dipole with T-matched circuit. (b) Conventional printed dipole RCS versus frequency. (c) Conventional printed dipole CMF versus frequency. (d) Radiation pattern of printed dipole with T-matched circuit at 0.875 GHz. (e) Conjugate match gain of printed dipole with T-matched circuit versus frequency. (f) Radiation efficiency of printed dipole with T-matched circuit versus frequency.

5.2. Meander Dipole

Table 1 shows the values of h_m for resonant frequency $f_o = 900\,\text{MHz}$. Meander Dipole Antenna (MDA) with $S_m = 72.6\,\text{mm}$ $b_m = 1\,\text{mm}$, $W_m = 18\,\text{mm}$, $m = 2$ and h_m will be in the rang from 28 mm to 30 mm. Due to the transformation from wire structure to planar structure, h_m is optimized a little bit and found to be 30.5 mm as shown in Fig. 11(a). Using IE3D simulator, the input impedance of MDA versus frequency could be obtained as shown in Fig. 11(b) and found to be $19.75 - \text{j}4.6\,\Omega$ at 900 MHz. T-matched circuit chart is used as shown in Fig. 11(c) which indicates that the matched condition to the chip input impedance of $13.9-\text{j}143.6$ is hard to be obtained. So as a starting point let us begin with $b/w = 3.5$ and $a_d/l = 0.045$. T-matched chart indicates that the input impedance will be $22.96 + \text{j}37\Omega$ as shown in Fig. 11(c). IE3D simulator is used to confirm the result as shown in Fig. 11(d) where the structure with T-matched section is simulated, and its input impedance versus frequency is shown in Fig. 11(e). As shown in Fig. 11(e), MDA input impedance has the value of $23.288 + \text{j}36.36\,\Omega$ with $b/w = 3.5$ and $a_d/l = 0.03597 \approx 0.04$. A second T-matched section would be needed. IE3D simulator is used for the structure shown in Fig. 11(f) with $b/w = 4$ and $a_d/l = 0.077 \approx 0.08$.

Input impedance versus frequency is shown in Fig. 11(g). PRC of $13.9 - j143.6\Omega$ chip input impedance is shown in Fig. 11(h) which indicates that MDA covers the frequency band 895 MHz–963 MHz. RCS as shown in Fig. 11(i) indicates that at 900 MHz the antenna RCS is $0.0383\,m^2$ which reader could detect easily. As shown in

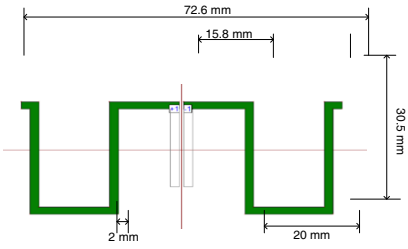

(a)

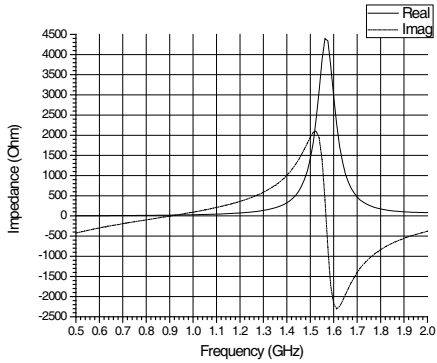

(b)

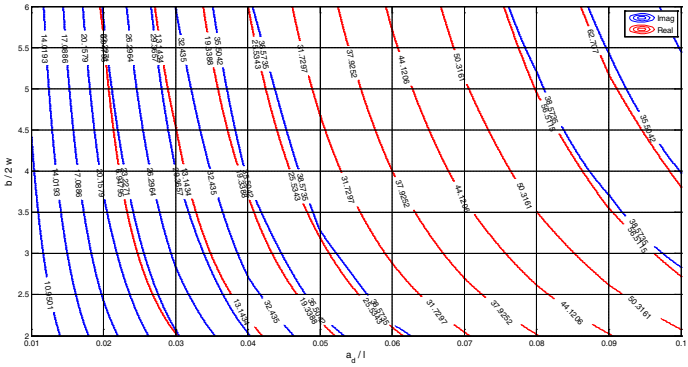

(c)

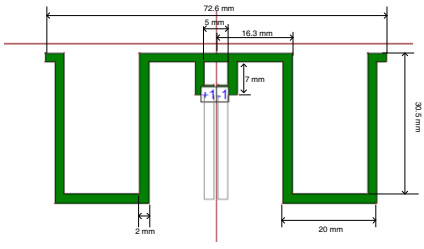

(d)

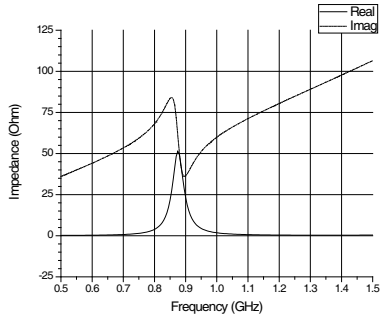

(e)

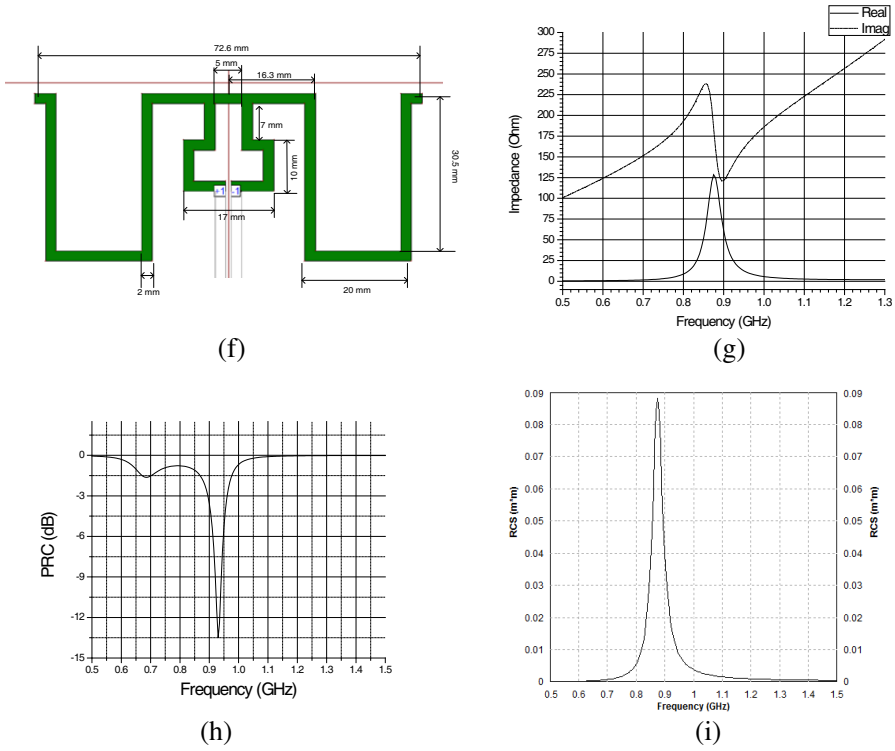

Figure 11. (a) Printed MDA structure. (b) Printed MDA input impedance versus frequency. (c) T-matched chart for MDA input impedance of $19.75 - j4.6\,\Omega$. (d) MDA with first T-matched section. (e) MDA with its first T-matched circuit section. (f) MDA with second T-matched section. (g) MDA input impedance versus frequency. (h) MDA PRC versus frequency. (i) MDA RCS versus frequency.

Fig. 12(a), CMF = 0.47 at 900 MHz which agrees with the T-matched chart for matching process difficulties. Fig. 12(b) shows the radiation pattern which is almost omnidirectional at the H-plane and the shape of 8 at the E-plane which makes this pattern very suitable for the RFID surveillance applications. Other antenna parameters such as conjugate match gain and radiation efficiency are shown in Fig. 12(c) and Fig. 12(d), respectively.

5.3. Franklin Dipole

For more compactness, we can use Franklin shape [19], thus get the same resonant frequency but with $h_m = 18$ mm. Following the same

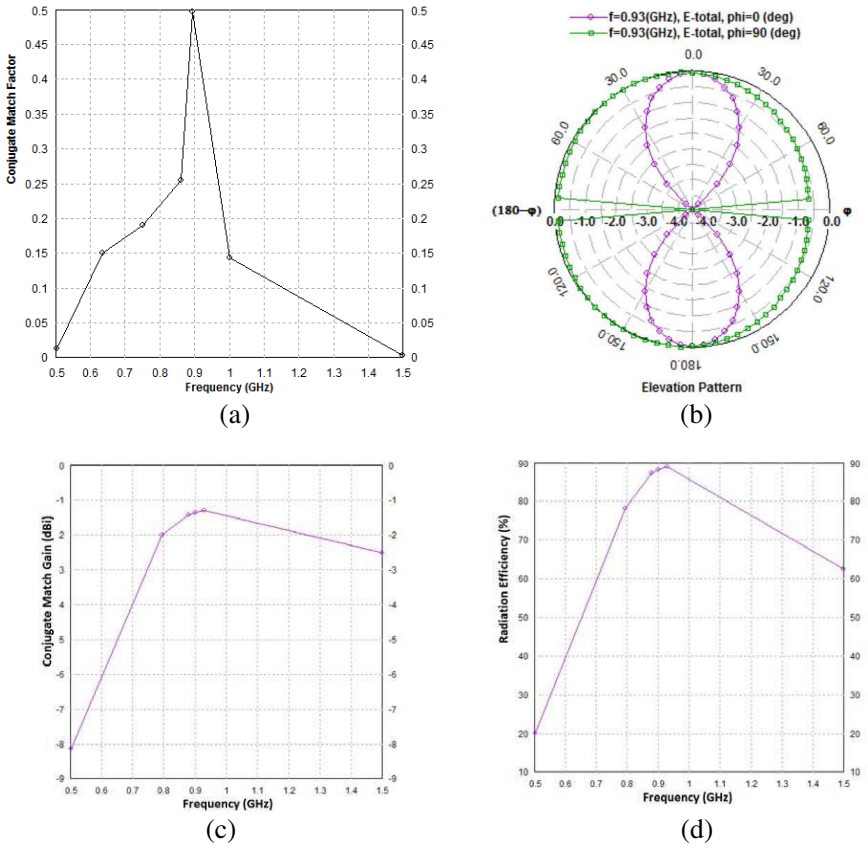

Figure 12. (a) MDA CMF versus frequency. (b) MDA radiation pattern at 930 MHz. (c) MDA conjugate match gain. (d) MDA conjugate radiation efficiency.

procedure, shown in Fig. 10, a Franklin shape dipole antenna was designed as shown in Fig. 13(a). The input impedance was calculated using IE3D EM simulator at 900 MHz and found to be $17.66 - \text{j}64.2\Omega$ as shown in Fig. 13(b). We used the input impedance to get the T-matched impedance chart as shown in Fig. 13(c), and it is found to be $14 + \text{j}119.5\Omega$ by choosing $b/w = 9$ and $a_d/l = 0.062$.

Using the IE3D simulator for the Franklin dipole shape with T-matched circuit, as shown in Fig. 14(a) by choosing $b/w = 8.875$ mm, $b/w' = 11.83$ mm and $a_d/l = 0.0485$ mm, the input impedance is found to be $6 + \text{j}145.3\,\Omega$. The input impedance versus frequency

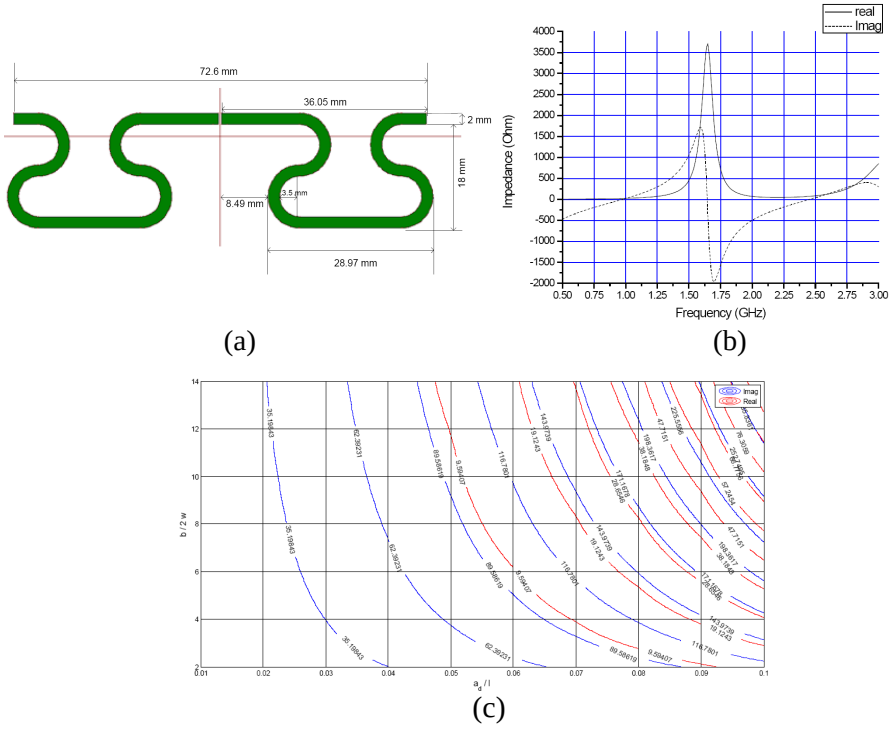

Figure 13. (a) Franklin shape dipole antenna. (b) Simulated Franklin shape dipole antenna input impedance versus frequency using IE3D simulator. (c) T-matched circuit chart for Franklin shape dipole with $17.66 - \text{j}642\,\Omega$ input impedance.

is shown in Fig. 14(b) and found to be $5.92 + \text{j}145.3\,\Omega$. The PRC for $13.9 - \text{j}143.6\,\Omega$ chip input impedance is shown in Fig. 14(c). It indicates that a frequency band from 865 MHz–1078 MHz is achieved. The obtained frequency band is suitable for the universal RFID UHF application. RCS shown in Fig. 14(d) indicates that at 900 MHz the antenna introduces RCS of $0.008\,\text{m}^2$. As shown in Fig. 14(e), CMF = 0.825 at 900 MHz which indicates that a good matched condition is obtained. Fig. 15(a) shows the radiation pattern which is almost omnidirectional at the H-plane and the shape of 8 at the E-plane which makes this pattern very suitable for RFID surveillance applications. Other antenna parameters such as conjugate match gain and radiation efficiency are shown in Fig. 15(c) and Fig. 15(d), respectively.

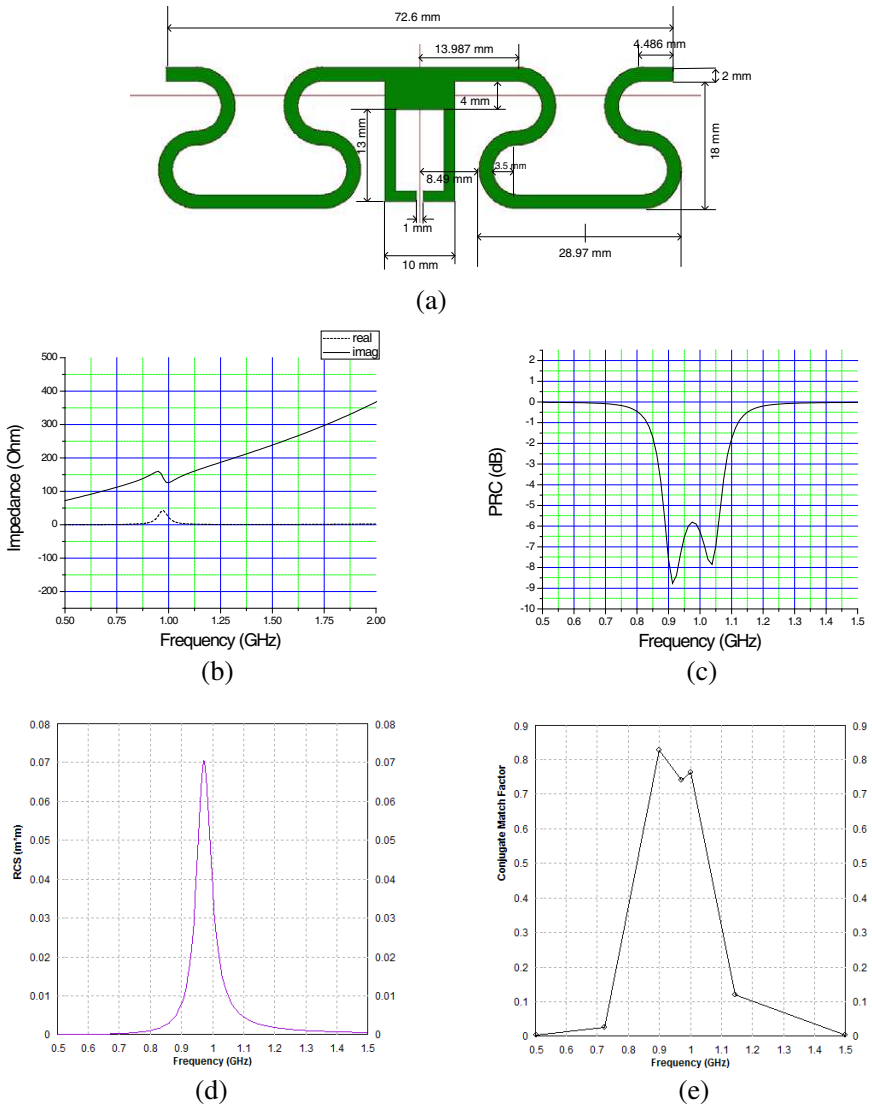

Figure 14. (a) Franklin shape dipole with $S_m = 72.6\,\text{mm}$, $b_m = 1\,\text{mm}$, $W_m = 18\,\text{mm}$ and $h_m = 18\,\text{mm}$. (b) Franklin dipole shape with T-match input impedance versus frequency. (c) PRC Franklin dipole shape with T-match versus frequency. (d) Franklin dipole shape RCS versus frequency. (e) Franklin dipole shape CMF versus frequency.

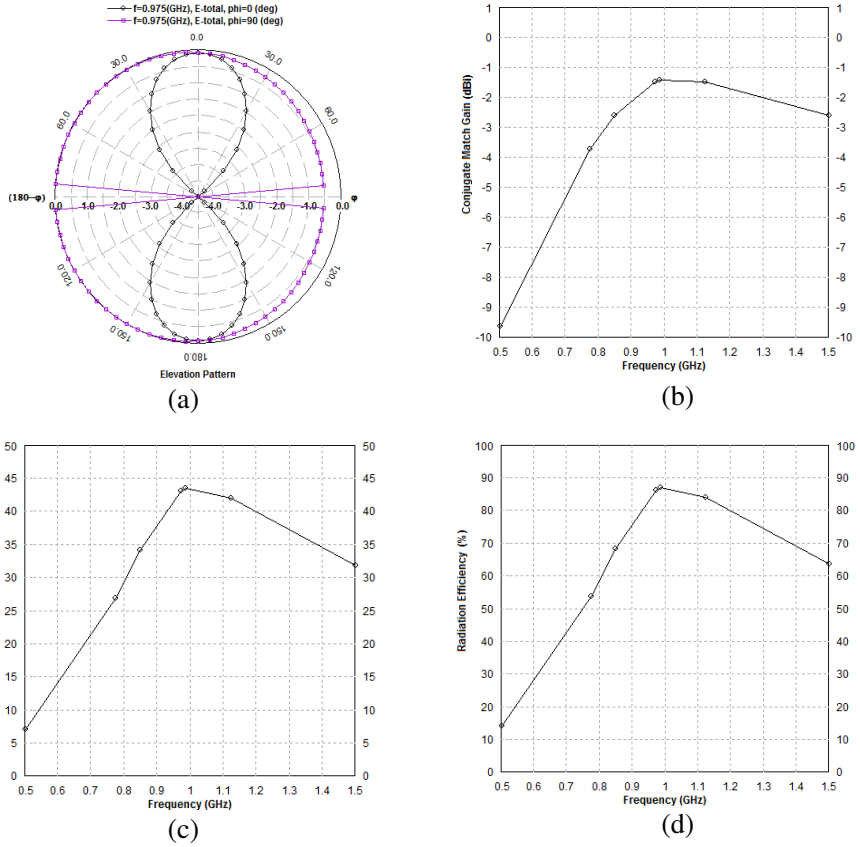

Figure 15. (a) Radiation pattern of Franklin shape dipole with T match circuit. (b) Conjugate match gain of Franklin shape dipole with T-matched circuit. (c) Conjugate match efficiency of Franklin shape dipole with T-matched circuit. (d) Radiation efficiency of Franklin shape dipole with T-matched circuit.

6. EXPERIMENTAL RESULTS

Franklin dipole antenna represents the most complex and thus the most interesting geometry, so it was fabricated using photolithographic technique on LCP copper clad substrate with $\varepsilon_r = 2.9$, thickness $h = 0.05\,\text{mm}$ and $\tan\delta = 0.0025$ as shown in Fig. 16. The simulated bandwidth covers the band of 870 MHz to 1080 MHz which is the universal UHF RFID frequency band. As shown in Fig. 17, PRCs

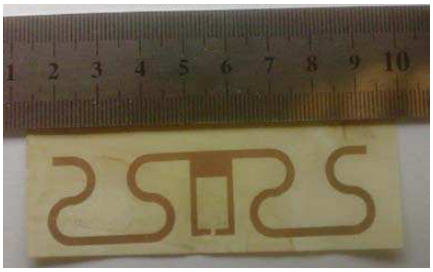

Figure 16. A photo of fabricated Franklin dipole shape over LCP substrate.

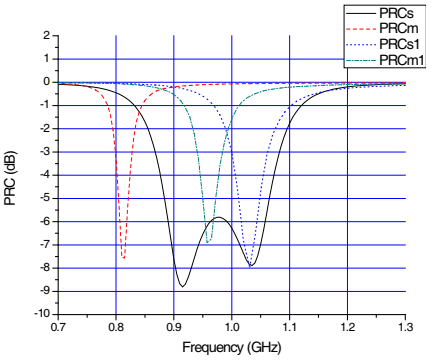

Figure 17. Simulated and measured PRC of the Franklin dipole shape.

is the simulated PRC for the whole Franklin shape dipole. PRCm is the measured PRC through measuring half structure of the Franklin shape dipole over a ground plane and multiplying the measured input impedance by two, and hence PRC is computed. Discrepancy between simulated and measured PRCs may be attributed to the flexible nature of the LCP substrate as well as that the gap between the half Franklin shape and the ground plane cannot be eliminated. So, we simulated the structure again but with a gap of 0.5 mm placed at the structure symmetrical plane. The resultant PRC is the PRCs1. Measurements are carried out again with a trial to reduce the gap as possible, and the resultant is PRCm1 which shows good agreement with the simulated results. The matching of the dipole input impedance to the chip impedance is given at certain frequency and free space. The impedance of the chip is a function of frequency and received power, and the impedance of the antenna is highly dependent on the support on which the tag is placed [20]. The ΔRCS is an important parameter when the passive tag is no longer in the expected configuration of use, for example when it is mounted on a disruptive, or it is physically deformed, or the reader operates at a frequency other than the tag's resonance. As specified in the ISO 18000-6 standard, the ΔRCS is greater than 50 cm^2 when output power is equal to 1.2 times the threshold power [21]. Furthermore, it decreases when the power increases. In this manner, the depth of modulation seen by the reader remains constant. The investigation of ΔRCS and backscattering will be good topics for future studies.

7. CONCLUSION

In this paper, induced EMF method was used to analyze and design three flexible UHF RFID antennas, namely conventional dipole antenna, meander dipole antenna and Franklin shape dipole antenna. A systematic design procedure chart was obtained. Derivation and verification of induced EMF dipole input impedance considering wire radius were introduced. We were aiming to reduce the tag antenna size. This was done through three steps namely, conventional printed dipole, rampart printed dipole, and Franklin printed dipole. In the second step, the conventional printed dipole was modified using the rampart shape. This step reduces the area by 11.16% and the length reduction by 56.43% as compared to the conventional flat dipole. The third step was using the Franklin shape for more size reduction. This step reduced the tag area by 4533% as compared to the conventional flat dipole. Also size reduction was achieved through the use of Franklin shape antenna since it occupies smaller area than previously published antennas. The proposed Franklin antenna covering the frequency band from 865 MHz to 1078 MHz insuring the UHF RFID universal frequency band tag applications. Computed radar cross section and conjugate match factor were introduced and discussed for the proposed antennas and insure that the proposed antennas structures are easily detectable and achieve acceptable matching level. Both computed and measured power reflection coefficients were investigated. Other antenna parameters such as radiation efficiency, gain and radiation pattern were found to be at acceptable level. The proposed Franklin designed antenna was fabricated, and its performance was measured. Good agreement was found between measured and simulated results. The proposed antennas are cheap, flexible and suitable for UHF RFID universal application.

REFERENCES

1. Abdallah, E. A., T. G. Abo-Elnaga, and H. M. El-Henawy, "Ground slotted phi shape UWB stacked circular polarized antenna for 5.8 GHz RFID reader," *PIERS Proceedings*, 230–234, Cambridge, USA, Jul. 5–8, 2010.
2. Abdallah, E. A., T. G. Abo-Elnaga, and H. M. El-Henawy, "Ground slotted landa shape single feed UWB circular polarized antenna for 2.4 GHz RFID reader," *PIERS Proceedings*, 225–229, Cambridge, USA, Jul. 5–8, 2010.
3. Abo-Elnaga, T. G., E. A. Abdallah, and H. M. El-Hennawy, "UWB circular polarization RFID reader antenna for 2.4 GHz

band," *PIERS Proceedings*, 882–886, Xi'an, China, Mar. 22–26, 2010.

4. Abo-Elnaga, T. G., E. A. Abdallah, and H. M. El-Hennawy, "Universal UHF RFID rose reader antenna," *PIERS Proceedings*, 870–874, Xian, China, Mar. 22–26, 2010.
5. Yao, Y., Y. Sui, X. Chen, and J. Yu, "Planar antenna for RFID tags on metal platform," *IEEE International Workshop on Antenna Technology (IWAT)*, 408–411, 2011.
6. Son, H. W. and S. H. Jeong, "Wideband RFID tag antenna for metallic surfaces using proximity-coupled feed," *IEEE Antennas and Wireless Propagation Letters*, Vol. 10, 377–380, 2011.
7. Lee, S., H. Jung, H. Choo, and I. Park, "Design of a u-shaped RFID tag antenna with an isotropic radiation characteristic," *International Workshop on Antenna Technology (IWAT)*, 306–309, 2011.
8. Kim, D. and J. Yeo, "Low-profile RFID tag antenna using compact AMC substrate for metallic objects," *IEEE Antennas and Wireless Propagation Letters*, Vol. 7, 718–720, 2008.
9. Ukkonen, L., L. Sydänheimo, and M. Kivikoski, "Effects of metallic plate size on the performance of microstrip patch-type tag antennas for passive RFID," *IEEE Antennas and Wireless Propagation Letters*, Vol. 4, 410–413, 2005.
10. Yang, L., S. Basat, and M. Tentzeris, "Design and development of novel inductively coupled RFID antennas," *IEEE Antennas and Propagation Society International Symposium*, 1035–1038, Jul. 2006.
11. Ukkonen, L., M. Schaffrath, J. A. Kataja, L. Sydanheimo, and M. Kivikoski, "Evolutionary RFID tag antenna design for paper industry applications," *International Journal of Radio Frequency Identification Technology and Applications*, 107–122, Jan. 2006.
12. Balanis, C. A., *Antenna Theory Analysis and Design*, John Wiley & Sons, Inc., 2005.
13. Abramowitz, M., *Handbook of Mathematical Function*, Dec. 1972.
14. Hu, Z., P. H. Cole, and L. Zhang, "A method for calculating the resonant frequency of meander-line dipole antenna," *Industrial Electronics and Applications (ICIEA) Conference*, 1783–1786, Xian, May 2009.
15. Marrocco, G., "The art of UHF RFID antenna design, impedance-matching and size-reduction techniques," *IEEE Antennas and Propagation Magazine*, Vol. 50, No. 1, 66–79, Feb. 2008.

16. Chu, Q. X., L. Wang, and J. K. Zhou, "A novel folded T-matched dipole in base station," *Int. Conf. Microwave and Millimeter Wave Technology (ICMMT'07)*, 1–3, 2007.
17. Butler, C. H., "The equivalent radius of a narrow conducting strip," *IEEE Trans. Antennas Propagation*, Vol. 30, No. 4, 755–758, Jul. 1982.
18. Alien Higgs-2 EPC global Class 1 Gen 2 UHF RFID tag IC product overview, Alien Technology, 18220 Butterfield Blvd. Morgan Hill, ww.alientechnology.com.
19. Nishimja, S., K. Nakaro, and T. Makimoto, "Franklin type microstrip line antenna," *IEEE Antennas and Propagation Society International Symposium*, Vol. 17, 134–137, 1979.
20. Pillai, V., "Impedance matching in RFID tags: To which impedance to match?," *IEEE Antennas and Propagation International Symposium,* 3505–3508, Jun. 2006.
21. Pouzin, A., T. Vuong, S. Tedjini, M. Pouyet, and J. Perdereau, "Measurement of differential radar cross section of UHF RFID tags," *PIERS Proceedings*, 1232–1234, Moscow, Russia, Aug. 2009.